International Journal of Innovative Technology and Exploring Engineering (IJITEE)
ISSN: 2278-3075 (Online), Volume-4 Issue-7, December 2014

High Step-Up DC–DC Converter for AC Photovoltaic Module Application

Ponugoti Sri Lakshmi, Kande Dayakar, Dola Sanjay S

Abstract*— Photovoltaic (PV) power-generation market of ac PV module has shown obvious growth. However, a high voltage gain converter is essential for the module's grid connection through a dc–ac inverter. This paper proposes a converter that employs a floating active switch to isolate energy from the PV panel when the ac-module is OFF; this particular design protects installers and users from electrical hazards. Without extreme duty ratios and the numerous turns-ratios of a coupled inductor, this converter achieves a high step-up voltage-conversion ratio; the leakage inductor energy of the coupled inductor is efficiently recycled to the load. These features explain the module's high-efficiency performance. The detailed operating principles and steady-state analyses of continuous, discontinuous modes are described. A 15V input voltage, 200V output voltage, 100W output power proto type circuit of the proposed converter has been implemented; its maximum efficiency is up to 95.3% and full-load efficiency is 92.3%.

***Index Terms*—AC module, coupled inductor, high step-up voltage gain, single switch.**

I. INTRODUCTION

PHOTOVOLTAIC (PV) power-generation systems are be- coming increasingly important and prevalent in distribution generation systems. A conventional centralized PV array is a serial connection of numerous panels to obtain higher dc-link voltage for main electricity through a dc–ac inverter [1], [30]. Unfortunately, once there is a partial shadow on some panels, the system's energy yield become significantly reduced[2].An ac module is a micro inverter configured on the rear bezel of a PV panel [1]–[3]; this alternative solution not only immunizes against the yield loss by shadow effect, but also provides flexible installation accordance with the user's budget[4]. Many prior research works have proposed a single-stage dc– ac inverter with fewer components to fit the dimensions of the bezel of the ac module, but their efficiency levels are lower than those of conventional PV inverters. The power capacity a single PV panel is about 100W to 300W, and the maxi- mum power point (MPP) voltage range is from 15V to 40V, which will be the input voltage of the ac module; in cases with lower input voltage, it is difficult for the ac module to reach high efficiency [3]. However, employing a high step-up dc–dc converter in the front of the inverter improves power conversion efficiency and provides a stable dc link to the inverter.

Manuscript published on 30 December 2014.
*Correspondence Author(s)
Ponugoti Srilakshmi , Electrical & Electronics Engg, JNTU Anantapur University, Geethanjali institute of science & technology, SPSR Nellore, India.
Asst.Prof. Kande Dayakar , Electrical & Electronics Engg ,JNTU Anantapur University, Geethanjali institute of science & technology, SPSR Nellore , India, k. Dayakar
Prof. Dola Sanjay S, Electronics & Communication Engg, Atmakur Engineering College, Atmakur, India.

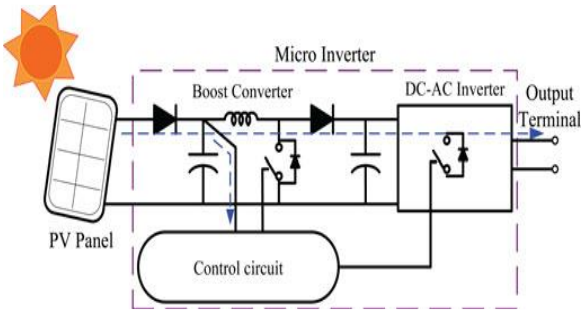

Fig.1. Potential difference on the output terminal of non floating switch micro inverter.

Fig. 1 shows the solar energy through the PV panel and micro inverter to the output terminal when the switches are OFF. When installation of the ac module is taking place, this potential difference could pose hazards to both the worker and the facilities. A floating active switch is designed to isolate the dc current from the PV panel, for when the ac module is off-grid as well as in the non operating condition. This isolation ensures the operation of the internal components without any residential energy being transferred to the output or input terminals, which could be unsafe. The micro inverter includes dc–dc boost converter, dc–ac inverter with control circuit as shown in Fig. 1.

The dc–dc converter requires large step-up conversion from the panel's low voltage to the voltage level of the application Previous research on various converters for high step-up applications has included analyses of the switched-inductor and switched-capacitor types[6],[7];transformer less switched - capacitor type [8], [9], [29]; the voltage-lift type [12]; the capacitor-diode voltage multiplier [13]; and the boost type integrated with a coupled inductor [10], [11], these converters by increasing turns ratio of coupled inductor obtain higher voltage gain than conventional boost converter. Some converters successfully combined boost and fly back converters, since various converter combinations are developed to carry out high step-up voltage gain by using the coupled-inductor technique [14]–[19],[27],[28].

The efficiency and voltage gain of the dc–dc boost converter are constrained by either the parasitic effect of the power switches or the reverse-recovery issue of the diodes. In addition, the equivalent series resistance (ESR) of the capacitor and the parasitic resistances of the inductor also affect overall efficiency. Use of active clamp technique not only recycles the leakage inductor's energy but also constrains the voltage stress across the active switch, how- ever the tradeoff higher cost and complex control circuit[25], [26]. By combining active snubber auxiliary resonant circuit, synchronous rectifiers, or switched- capacitor-based resonant circuits and soon ,

these techniques made active switch into zero voltage switching (ZVS) or zero current switching (ZCS) operation and improved converter efficiency [20]–[24]. However, when the leakage- inductor energy from the coupled inductor can be recycled, the voltage stress on the active switch is reduced, which means the coupled inductor employed in combination with the voltage-multiplier or voltage-lift technique successfully accomplishes the goal of higher voltage gain [6]–[13]

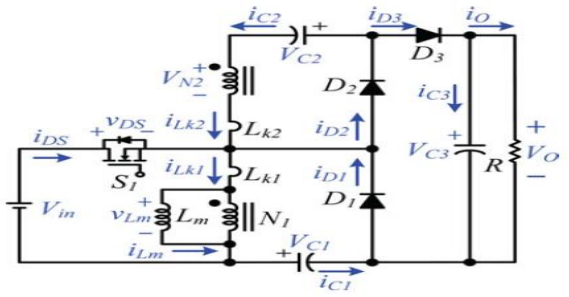

Fig. 2. Circuit configuration of proposed converter

The proposed converter, shown in Fig. 2, is comprised of a coupled inductor T_1 with the floating active switch S_1. The primary winding N_1 of a coupled inductor T_1 is similar to the input inductor of the Conventional boost converter, and capacitor C_1 and diode D_1 receive leakage inductor energy from N_1.The secondary winding N_2 of coupled inductor T_1 is connected with another pair of capacitors C_2 and diode D_2, which are in series with N_1 in order to further enlarge the boost voltage. The rectifier diode D_3 connects to its output capacitor C_3

The proposed converter has several features:

1) The connection of the two pairs of inductors, capacitor, and diode gives a large step-up voltage-conversion ratio

2) The leakage-inductor energy of the coupled inductor can be recycled, thus increasing the efficiency and restraining the voltage stress across the active switch

3) The floating active switch efficiently isolates the PV panel energy during non operating conditions, which enhances safety. The operating principles and steady-state analysis of the proposed converter are presented in the following sections

II. OPERATING PRINCIPLES OF THE PROPOSED CONVERTER

The simplified circuit model of the proposed converter is shown in Fig.2. The coupled inductor T_1 is represented as a magnetizing inductor L_m, primary and secondary leakage inductors L_{k1} and L_{k2}, and an ideal transformer. In order to simplify the circuit analysis of the proposed converter, the following assumptions are made.

1) All components are ideal, except for the leakage inductance of coupled inductor T_1, which is being taken under consideration. The on-state resistance $R_{DS}(ON)$ and all parasitic capacitances of the main switch S_1 are neglected, as are the forward voltage drops of diodes $D_1 \sim D_3$.

2) The capacitors $C_1 \sim C_3$ are sufficiently large that the voltages across them are considered to be constant.

3) The ESR of capacitors $C_1 \sim C_3$ and the parasitic resistance of coupled inductor T_1 are neglected.

4) The turn's ratio n of the coupled inductor T_1 windings is equal to N_2/N_1.

The operating principle of continuous conduction mode (CCM) is presented with the figures and current wave forms for continuous mode of operation as in figure 8. Here five modes of operation described with neat diagrams

A.CCM Operation

Mode I [t_0,t_1]: In this transition interval ,the magnetizing inductor Lm continuously charges capacitor C_2 through T_1 when S_1 is turned ON. The current flow path is shown in Fig.3 switch S_1 and diode D_2 is conducting. The current i_{Lm} is decreasing because source voltage V_{in} crosses magnetizing inductor L_m and primary leakage inductor L_{k1}; magnetizing inductor L_m is still transferring its energy through coupled inductor T_1 to charge switched capacitor C_2, but the energy is decreasing; the charging current i_{D2} and i_{C2} are decreasing. The secondary leakage inductor current i_{LK2} is declining as equal to i_{Lm} / n. Once the increasing i_{Lk1} equals decreasing i_{Lm} at t = t_1, this mode ends.

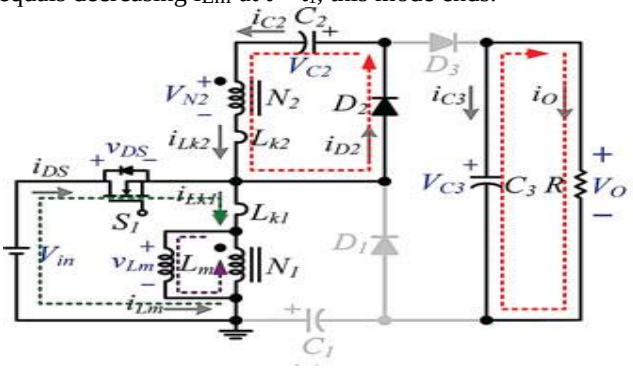

Fig. 3 current flowing from t_0 to t_1 in CCM

Mode II [t_1, t_2]: During this interval, source energy Vin is series connected with N_2, C_1 and C_2 to charge output capacitor C_3 and load R; meanwhile magnetizing inductor L_m is also receiving energy from V_{in}. The current flow path is shown in Fig.4, where switch S_1 remains ON and only diode D_3 is conducting. The i_{Lm}, i_{Lk1}, and i_{D3} are increasing because the V_{in} is crossing L_{k1}, L_m, and primary winding N_1; L_m and L_{k1} are storing energy from V_{in}; meanwhile V_{in} is also serially connected with secondary winding N_2 of coupled indutorssT_1, capacitors C_1, and C_2, and then discharges their energy to capacitor C_3 and load R. Then, i_{D3} and discharging current $|i_{C1}|$ and $|i_{C2}|$ are increasing. This mode ends when switch S_1 is turned OFF at t = t_2.

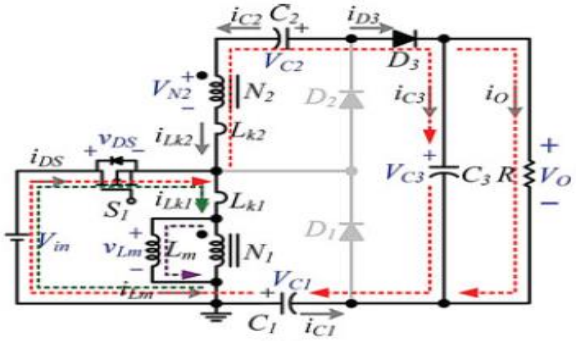

Fig. 4 current flowing fromt_1 to t_2 in CCM

Mode III [t_2, t_3]: During this transition interval, secondary leakage inductor L_{k2} keeps charging C_3 when switch S_1 is OFF. The current flow path is shown in Fig.5 where only diode D_1 and D_3 are conducting. The energy stored in leakage inductor L_{k1} flows through diode D_1 to charge capacitor C_1 instantly when S_1 is OFF.

Published By:
Blue Eyes Intelligence Engineering
and Sciences Publication (BEIESP)

Meanwhile, the energy of secondary leakage inductor L_{k2} is series connected with C_2 to charge output capacitor C_3 and the load. Because leakage inductance L_{k1} andL_{K2} are far smaller than Lm,i_{Lk2} rapidly decreases ,but i_{Lm} is increasing because magnetizing inductor Lm is receiving energy from L_{k1}. Current i_{Lk2} decreases until it reaches zero; this mode ends at t=t_3.

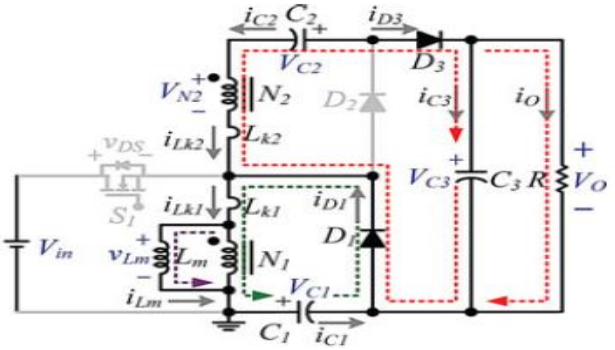

Fig. 5 current flowing fromt_2 to t_3 in CCM

Mode IV [t_3, t_4]: During this transition interval, the energy stored in magnetizing inductor Lm is released to C_1 and C_2 simultaneously. The current flow path is shown in Figure6. Only diodes D_1 and D_2 are conducting. Currents i_0.and i_{D1} are continually decreased because the leakage energy still flowing through diodeD_1 keeps charging capacitorC_1 .The Lm is delivering its energy through T_1 and D_2 to charge capacitor C_2. The energy stored in capacitor C_3 is constantly discharged to the load R. These energy transfers result in decreases in $i_{Lk1}$and i_{Lm} but increases in i_{Lk2}. This mode ends when current i_{Lk1} is zero at t=t_4

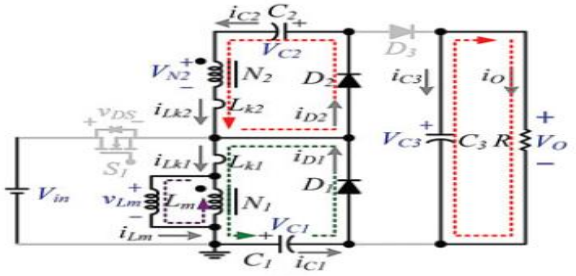

Fig. 6 current flowing from t_3 to t_4 in CCM

Mode V [t_4, t_5]: During this interval, only magnetizing inductor L_m is constantly releasing its energy to C_2. The current flow path is shown in Figure7 which only diode D_2 is con- ducting. The i_{Lm} is decreasing due to the magnetizing inductor energy flowing through the coupled inductor T_1 to secondary winding N_2, and D_2 continues to charge capacitor C_2. The energy stored in capacitor C_3 is constantly discharged to the load R. This mode ends when switch S_1 is turned ON at the beginning of the next switching period.

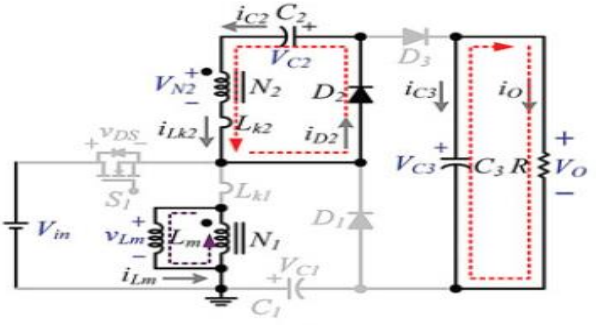

Fig. 7 current flowing from t_4 to t_5 in C CM

B. DCM Operation

The detailed operating principles for discontinuous-conduction-mode (DCM)operation represented in this section.

Fig14. Shows typical waveforms during five operating modes of one switching period. The operating modes are described as follows.

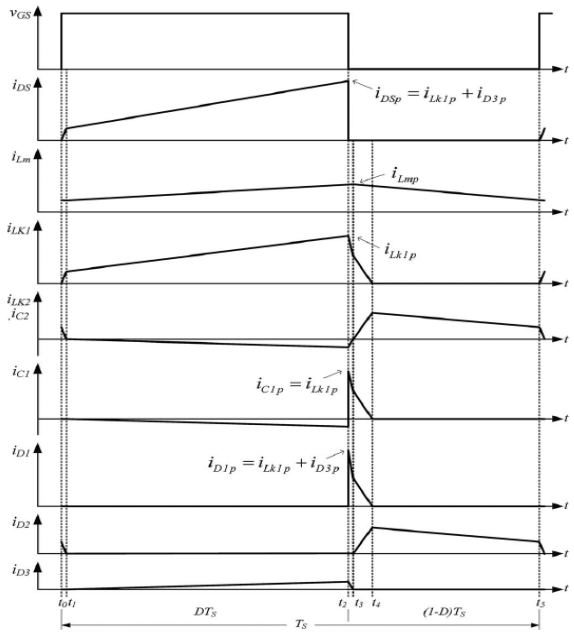

Fig. 8. Some typical waveforms of proposed converters at CCM operation

Mode I [t_0, t_1]: During this interval, source energy V_{in} is series connected with N_2,C_1,andC_2 to charge output capacitor C_3 and load R; meanwhile, magnetizing inductor Lm is also receiving energy from V_{in}. The current flow path is shown in Figure9, which depicts that switch S_1 remains ON, and only diode D_3 is conducting. The i_{Lm}, i_{Lk1}, and i_{D3} are increasing because the V_{in} is crossing L_{k1}, L_m, and primary winding N_1; L_m and L_{k1} are storing energy from V_{in}; meanwhile, V_{in} also is serially connected with secondary winding N_2 of coupled inductor T_1,capacitors C_1 and C_2 then they all discharge their energy to capacitorC_3 and load R .The iin,i_{D3} and discharging current $|i_{C1}|$ and $|i_{C2}|$ are increasing. This mode ends when switch S_1 is turned OFF at t = t1.

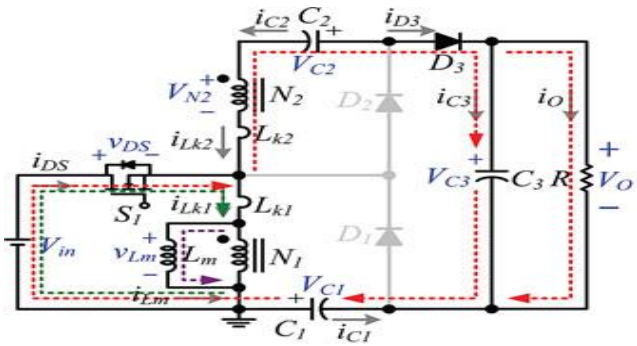

Fig. 9 current flowing from t_0 to $t_1$in DCM

Published By:
Blue Eyes Intelligence Engineering
and Sciences Publication (BEIESP)

Mode II [t_1, t_2]: During this transition interval, secondary leakage inductor L_{k2} keeps charging C_3 when switch S_1 is OFF. The current flow path is shown in Figure10, and only diode D_2 and D_3 are conducting. The energy stored in leakage inductor L_{k1} flows through diode D_1 to charge capacitor C_1 instantly when S_1 is OFF. Meanwhile, the energy of secondary leakage inductor L_{k2} is series-connected with C_2 to charge output capacitor C_3 and the load. Because leakage inductance L_{k1} andL_{K2} arefarsmallerthanLm,i_{Lk2} decreases rapidly ,but i_{Lm} is increasing because magnetizing inductor L_m is receiving energy from L_{k1}. Current i_{Lk2} reduces down to zero, and this mode ends at t = t2.

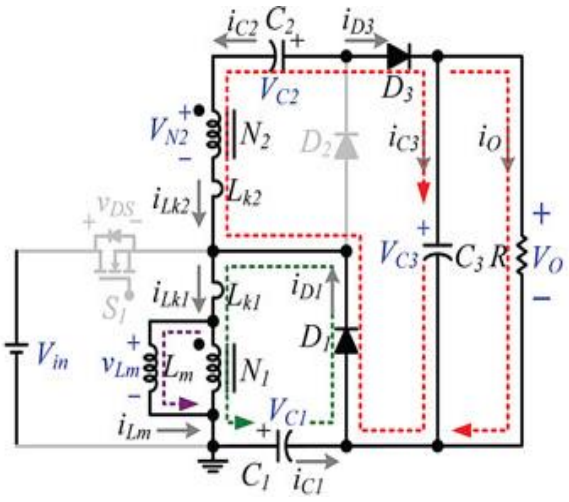

Fig. 10 current flowing from t_1 to t_2 in DCM

Mode III [t_2, t_3]: During this transition interval, the energy stored in coupled inductor T_1 is releasing to C_1 and C_2. The current flow path is shown in Fig11. Only diodesD_1 and D_2 are conducting. Currents i_{Lk1} and i_{D1} are continually decreased because leakage energy still flowing through diode D_1 keeps charging capacitor C_1. The L_m is delivering its energy throughT_1 and D_2 to charge capacitorC_2 .The energy stored in capacitor C_3constantly discharged to the load R. These energy transfers result in decreases in i_{Lk1} and i_{Lm} but increases in i_{Lk2}. This mode ends when current i_{Lk1} reaches zero at t = t_3.

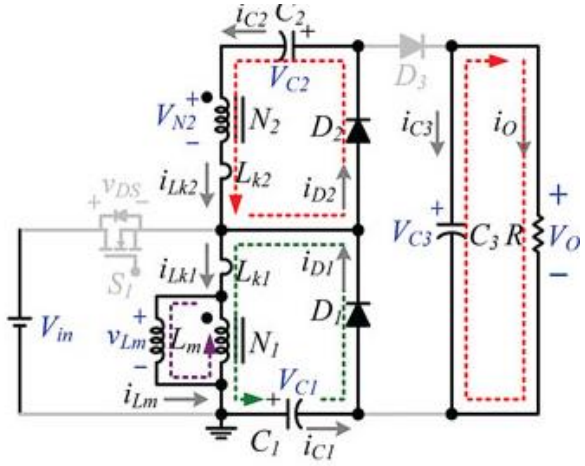

Fig. 11 current flowing from t_2 to t_3 in DCM

Mode IV [t_3, t_4]: During this interval only magnetizing inductor L_m is constantly releasing its energy to C_2. The current flow path is shown in Fig12 and only diodeD_2 is conducting. The i_{Lm} is decreasing due to the magnetizing inductor energy flowing through the coupled inductor T_1 to secondary wind- ing N_2, and D_2 continues to charge capacitor C_2. The energy stored in capacitor C_3 is constantly discharged to the load R. This mode ends when current i_{Lm} reaches zeroat t=t_4.

.

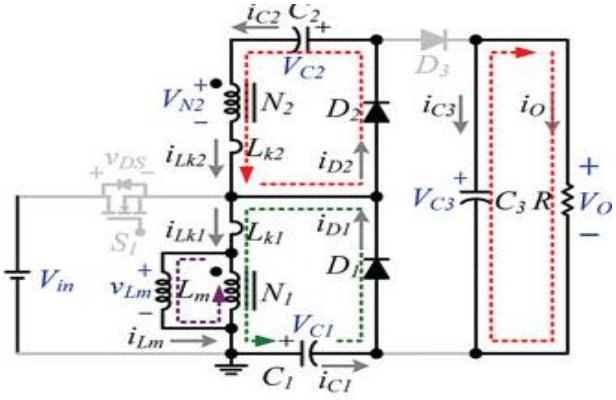

Fig. 12 current flowing from t_3 to t_4 in DCM

Mode V [t_4, t_5]: During this interval, all active components are turned OFF; only the energy stored in capacitor C_3 is con- tinued to be discharged to the load R. The current flow path is shown in Fig13 This mode ends when switch S1 is turned ON at the beginning of the next switching period.

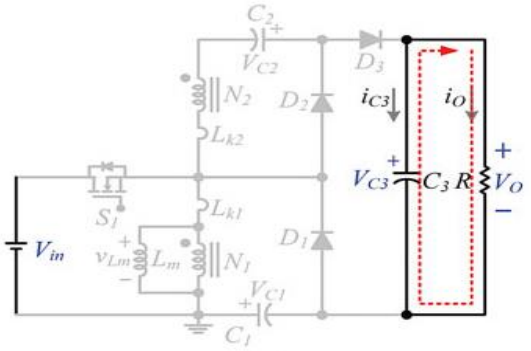

Fig. 13 current flowing from t_4 to t_5 in DCM

III. STEADY-STATE ANALYSIS OF PROPOSED CONVERTERS

A. Continuous-Conduction Mode (CCM)

In CCM, power transfer is a two-step process. When the switch is ON, stored energy builds in the inductor. When the switch is OFF, energy transfers to the output through the diode. The switch current is a stepped saw tooth with a fixed steady-state ON time with some amount of ripple current superimposed. During the ON time of the switch, if we assume zero losses for the moment, the voltage across the inductor is approximately the input voltage; and the voltage across the rectifier is the capacitor, or output voltage. When the switch turns OFF, the energy stored in the inductor releases into the output through the rectifier.

Published By:
Blue Eyes Intelligence Engineering and Sciences Publication (BEIESP)

The voltage across the inductor is approximately the input-to-output voltage difference, and the voltage across the switch becomes approximately the output voltage Important to any model is the understanding of the current in each of the relevant components in the power path. The mathematical construction of these currents helps to determine the magnitude and shapes of these currents. With zero losses assumed, the inductor current's ON-time slope is

$$m_{I_{L(ON)}} = \frac{V_{IN}}{L} \quad (1)$$

During the OFF time, the current will have a slope of

$$m_{IL(OFF)} = \frac{V_{IN-V_{OUT}}}{L} \quad (2)$$

If the V•s during the ON time of the switch is equated with theV•s during the OFF time of the switch,
Solving for the switch duty cycle, D, results in

$$\frac{V_{IN}}{L} \times D \times T_S = \frac{V_{IN-V_{OUT}}}{L} \times (1 - D) \times T_S \quad (3)$$

$$D_{CMM(ideal)} = 1 - \frac{V_{IN}}{V_{OUT}} \quad (4)$$

Power-stage input and output losses that impact the duty cycle are shown in Fig. The input losses include the inductor winding resistance (RL), the switch MOSFET RDS(ON), and (in the case of a current-mode-controlled converter) a current sense resistor (RISENSE). The output losses are represented by the output diode rectifier, D1.

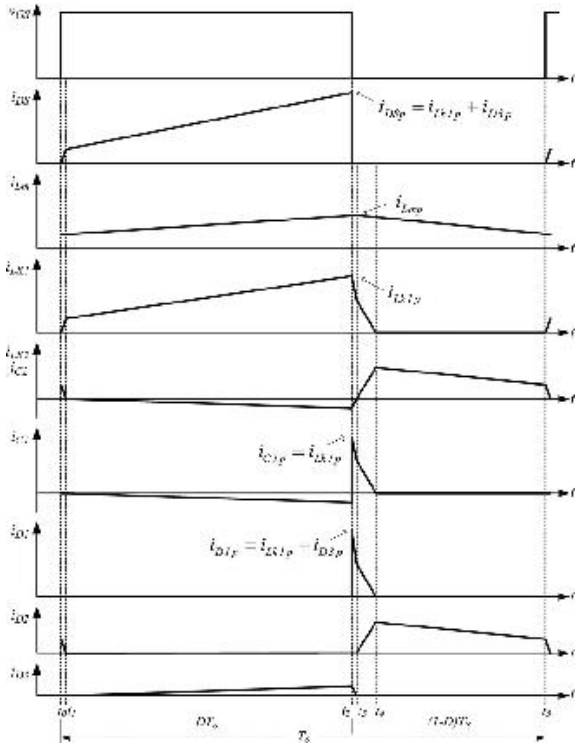

Fig. 14 Some typical waveforms of proposed converters at DCM operation

If the loss elements of the power-stage components are included, the equation for the duty cycle in CCM is shown by Equation above. This Equation holds true for CCM when the ripple current in the inductor is small relative to the average DC current. The equation is "close" when there is a high percentage of ripple current. Reassuringly, if the losses in Equation reduce to zero, the equation simplifies to the ideal case.

B. Discontinuous-Conduction Mode (DCM)

In DCM, a switching cycle is composed of three intervals. The first two are the same as in CCM, where energy is stored in the inductor during the ON time of the switch, and transferred to the load during the OFF time of the switch. In DCM, however, all of the energy in the inductor transfers to the load during this second interval. The third interval begins when the energy in the inductor is depleted, and terminates at the end of the switching period the next time the switch turns on. During this third interval the voltage across the inductor decays to zero, the voltage across the switch decays to the input voltage, and the in output voltage differential is across the rectifier. There is essentially no current flowing in the power stage during this interval.

Observe that since all of the energy in the inductor discharges in each switching cycle during an interval shorter than the (1 – D) conduction time, the peak current in the diode must be higher in DCM than in CCM. If the peak current is higher in the diode in DCM, then the peak current will be higher in the inductor and in the switch as well. With higher peaks and the same or a shorter conduction time, as a rule of thumb we can assume that for the same components, the RMS losses will be greater in a DCM converter than in an equivalent CCM converter.

The operating duty cycle of the converter in DCM dependent not only on the input and output voltages but on the inductor value and load current as well. In addition, in DCM operation, the current fall time (to zero) is usually different than (1 – D) x Ts. To find the duty cycle in DCM, we can first find the fall time that is required to discharge the inductor by taking the peak current during the ON time and dividing it by the current's rate of decay during the OFF time:

$$t_{fall} = \frac{m_{IL(ON)}}{-m_{IL(OFF)}} \times D \times T_S \quad (5)$$

The negative sign in the denominator of tf_{all} is due to the OFF-time slope being a negative value. If t_{fall} is less than (1 – D) x Ts, the converter is operating in DCM. That is, if the time to discharge the energy in the inductor to zero is less than the OFF time of the switch, the converter is operating in DCM. Under this condition, the fall-time duty cycle, D_{disch}, is

$$D_{disch} = \frac{t_{fall}}{T_S} = \frac{V_{IN}}{V_{OUT} - V_{IN}} \times D_{DCM} \quad (6)$$

In steady-state operation, the average output current is equal to the average diode current. This average output current is equal to the peak current, averaged over the switching period

Published By:
Blue Eyes Intelligence Engineering
and Sciences Publication (BEIESP)

$$I_{OUT} = \frac{V_{IN}}{2L} \times T_S \times D_{DCM} \times D_{disch} \quad (7)$$

Solving for the DCM duty cycle results in

$$D_{DCM} = \frac{1}{V_{IN}} \sqrt{\frac{2L \times (V_{OUT} - V_{IN})}{T_S}} \times \sqrt{I_{OUT}} \quad (8)$$

If losses are included, the following is a slightly better approximation

$$D_{DCM} = \frac{1}{V_{IN} - \frac{((V_{OUT}+V_d)\times I_{OUT}}{V_{IN}} \times R_{tot}} \times \sqrt{\frac{2L\times(V_{OUT}+V_d+V_{IN})}{T_S}} \times I_{OUT} \quad (9)$$

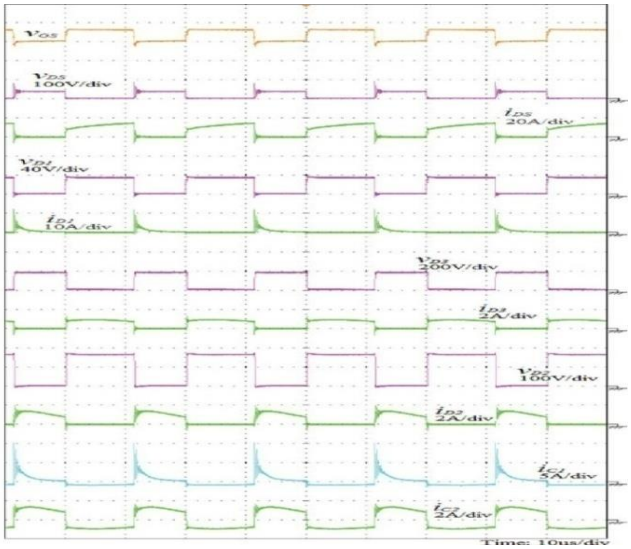

Fig15. Experimental waveforms measured by the condition of fS= 50 kHz, Vin=15 V, and output 100.

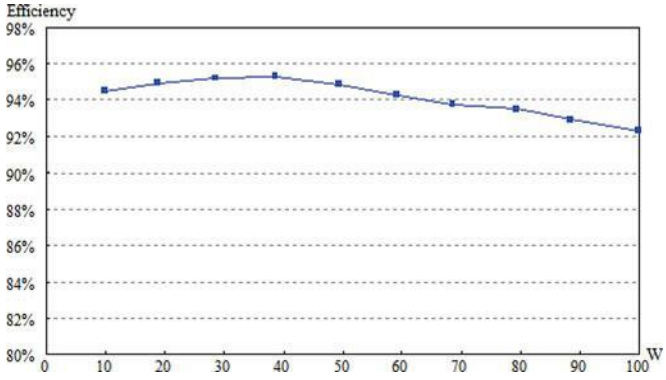

Fig. 16. Measured efficiency of proposed converter

III. EXPERIMENTALRESULTS

A 100W prototype sample is presented to verify the practicability of the proposed converter. The electrical specifications are V_{in} = 15V, VO = 200V, f_S = 50kHz, and full-load resistance R = 400 Ω.

The major components required are C1 = C2 = 47 μF and C3 = 220 μF. The main switch S_1 is a MOSFET IXFK180N15P, the diodes D_1 are MRB20200CTG , and the DPG30C300HB is selected for D_2 and D_3. Since assign turns ratio n = 5, the duty ratio D is derived as 55%.

The boundary normalized magnetizing inductor time constant τ_{LB} is found by to be 1.547×10−3. To define the proposed converter's BCM operation at 50% of the full load, the load resistance R = 800 Ω.

The boundary magnetizing inductance L_{mB} is found as follows: $L_{mB} \cdot f_S$ R > 1.547∗10−3 ⇒ L_m > 24.75 μH.

The actual inductance of magnetizing inductor Lm of the coupled inductor is 30.54 μH, which is larger than boundary magnetizing inductance 24.75μH. figure 15 shows voltage and current waveforms, which are measured from active switch S_1, diodes D_1, D_2, and D_3, and the current waveforms of C_1 and C_2. The measured voltage spike across the active switch is found to be about 80V; this reveals that the energy of the leakage inductor has been stored in and voltage clamped by C_1.

These experimental waveforms agree with the operating principles and the steady-state analysis. Fig. 16 shows that the maximum efficiency of 95.3% occurred at 40% of full load; and the full-load efficiency is maintained at 92.3% The efficiency variation is about 3%, and the flat efficiency curve is able to yield higher energy from the PV module during periods when sunlight is fading. The residential voltage discharge time of the proposed converter is 480 milliseconds, which prevents any potential electrical injuries to humans.

IV. CONCLUSION

Since the energy of the coupled inductor's leakage inductor has been recycled, the voltage stress across the active switch S_1 is constrained, which means low ON-state resistance $R_{DS(ON)}$can be selected. Thus, improvements to the efficiency of the proposed converter have been achieved. The switching signal action is performed well by the floating switch during system operation; on the other hand, the residential energy is effectively eliminated during the non operating condition, which improves safety to system technicians. From the prototype converter, the turns ratio *n* = 5 and the duty ratio *D* is 53%; thus, without extreme duty ratios and turns ratios, the proposed converter achieves high step-up voltage gain, of up to 13 times the level of input voltage. The experimental results show that the maximum efficiency of 94% is measured at half load, and a small efficiency variation will harvest more energy from the PV module during fading sunlight.

REFERENCES

1. T. Shimizu, K. Wada, and N. Nakamura, "Flyback-type single-phase utility interactive inverter with power pulsation decoupling on the dc input for an ac photovoltaic module system," *IEEE Trans. Power Electron.*, vol. 21, no. 5, pp. 1264–1272, Jan. 2006.
2. C. Rodriguez and G. A. J. Amaratunga, "Long-lifetime power inverter for photovoltaic ac modules," *IEEE Trans. Ind. Electron.*, vol. 55, no. 7, pp. 2593–2601, Jul. 2008.
3. S. B. Kjaer, J. K. Pedersen, and F. Blaabjerg, "A review of single-phase grid-connected inverters for photovoltaic modules," *IEEE Trans. Ind. Appl.*, vol. 41, no. 5, pp. 1292–1306, Sep./Oct. 2005.

Published By:
Blue Eyes Intelligence Engineering and Sciences Publication (BEIESP)

4. J. J. Bzura, "The ac module: An overview and update on self-contained modular PV systems," in *Proc. IEEE Power Eng. Soc. Gen. Meeting*, Jul. 2010, pp. 1–3.
5. B. Jablonska, A. L. Kooijman-van Dijk, H. F. Kaan, M. van Leeuwen, G.
6. T. M. de Boer, and H. H. C. de Moor, "PV-PRIVE project at ECN, five years of experience with small-scale ac module PV systems," in *Proc. 20th*
7. *EurPhotovoltaic Solar Energy Conf.*, Barcelona, Spain, Jun. 2005,pp. 2728–2731.
8. T. Umeno, K. Takahashi, F. Ueno, T. Inoue, and I. Oota, "A new approach to low ripple-noise switching converters on the basis of switched- capacitor converters," in *Proc. IEEE Int. Symp. Circuits Syst.*, Jun. 1991, pp. 1077– 1080.
9. B. Axelrod, Y. Berkovich, and A. Ioinovici, "Switched-capacitor/ switched-inductor structures for getting transformer less hybrid dc–dc PWM converters," *IEEE Trans. Circuits Syst. I, Reg. Papers*, vol. 55, no. 2, pp. 687–696, Mar. 2008.
10. B. Axelrod, Y. Berkovich, and A. Ioinovici, "Transformerless dc–dc con-verters with a very high dc line-to-load voltage ratio," in *Proc. IEEE Int. Symp. Circuits Syst. (ISCAS)*, 2003, vol. 3, pp. 435–438.
11. H. Chung and Y. K. Mok, "Development of a switched-capacitor dc–dc boost converter with continuous input current waveform," *IEEE Trans. Circuits Syst. I, Fundam. Theory Appl.*, vol. 46, no. 6, pp. 756–759, Jun. 1999.
12. T. J. Liang and K. C. Tseng, "Analysis of integrated boost-flyback step-up converter," *IEE Proc. Electrical Power Appl.*, vol. 152, no. 2, pp. 217–225, Mar. 2005.
13. Q. Zhao and F. C. Lee, "High-efficiency, high step-up dc–dc converters," *IEEE Trans. Power Electron.*, vol. 18, no. 1, pp. 65–73, Jan. 2003.
14. M. Zhu and F. L. Luo, "Voltage-lift-type cuk converters: Topology and analysis," *IET Power Electron.*, vol. 2, no. 2, pp. 178–191, Mar. 2009.
15. J. W. Baek, M. H. Ryoo, T. J. Kim, D. W. Yoo, and J. S. Kim, "High boost converter using voltage multiplier," in *Proc. IEEE Ind. Electron. Soc. Conf. (IECON)*, 2005, pp. 567–572.
16. J.Xu, "Modeling and analysis of switching dc–dc converter with coupled-inductor," in *Proc. IEEE 1991 Int. Conf. Circuits Syst. (CICCAS)*, 1991, 717–720.
17. R. J. Wai, C. Y. Lin, R. Y. Duan, and Y. R. Chang, "High-efficiency dc–dc converter with high voltage gain and reduced switch stress," *IEEE Trans. Ind. Electron.*, vol. 54, no. 1, pp. 354–364, Feb. 2007.
18. S. M. Chen, T. J. Liang, L. S. Yang, and J. F. Chen, "A cascaded high step-up dc–dc converter with single switch for micro source applications," *IEEE Trans. Power Electron.*, vol. 26, no. 4, pp. 1146–1153, Apr. 2011.
19. T. J. Liang, S. M. Chen, L. S. Yang, J. F. Chen, and A. Ioinovici, "Ultra large gain step-up switched-capacitor dc–dc converter with coupled inductor for alternative sources of energy," *IEEE Trans. Circuits Syst. I*, to be published.
20. L. S. Yang and T. J. Liang, "Analysis and implementation of a novel bidirectional dc–dc converter," *IEEE Trans. Ind. Electron.*, vol. 59, no. 1, 422–434, Jan. 2012.
21. W. Li and X. He, "Review of non-isolated high-step-up dc/dc converters in photovoltaic grid-connected applications," *IEEE Trans. Ind. Electron.*, vol. 58, no. 4, pp. 1239–1250, Apr. 2011.
22. S. H. Park, S. R. Park, J. S. Yu, Y. C. Jung, and C. Y. Won, "Analysis and design of a soft-switching boost converter with an HI-Bridge auxiliary resonant circuit," *IEEE Trans. Power Electron.*, vol. 25, no. 8, pp. 2142– 2149, Aug. 2010.
23. G. Yao, A. Chen, and X. He, "Soft switching circuit for interleaved boost converters," *IEEE Trans. Power Electron.*, vol. 22, no. 1, pp. 80–86, Jan. 2007.
24. Y. Park, S. Choi, W. Choi, and K. B. Lee, "Soft-switched interleaved boost converters for high step-up and high power applications," *IEEETrans. Power Electron.*, vol. 26, no. 10, pp. 2906–2914, Oct. 2011.
25. Y. Zhao, W. Li, Y. Deng, and X. He, "Analysis, design, and experimentation of an isolated ZVT boost converter with coupled inductors," *IEEE Trans. Power Electron.*, vol. 26, no. 2, pp. 541–550, Feb. 2011.
26. H. Mao, O. Abdel Rahman, and I. Batarseh, "Zero-voltage-switching dc– dc converters with synchronous rectifiers," *IEEE Trans. Power Electron.*, vol. 23, no. 1, pp. 369–378, Jan. 2008.
27. J. M. Kwon and B. H. Kwon, "High step-up active-clamp converter with input-current doubler and output-voltage doubler for fuel cell power systems," *IEEE Trans. Power Electron.*, vol. 24, no. 1, p. 108–115, Jan. 2009.
28. S. Dwari and L. Parsa, "An efficient high-step-up interleaved dc–dc converter with a common active clamp," *IEEE Trans. Power Electron.*, vol. 26, no. 1, pp. 66–78, Jan. 2011.
29. C. Restrepo, J. Calvente, A. Cid, A. El Aroudi, and R. Giral, "A non-inverting buck-boost dc–dc switching converter with high efficiency and wide bandwidth," *IEEE Trans. Power Electron.*, vol. 26, no. 9, pp. 2490– 2503, Sep. 2011.
30. K. B. Park, G. W. Moon, and M. J. Youn, "Nonisolated high step-up boost converter integrated with sepic converter," *IEEE Trans. Power Electron.*, vol. 25, no. 9, pp. 2266–2275, Sep. 2010.
31. L. S. Yang, T. J. Liang, and J. F. Chen, "Transformerless dc–dc converters with high step-up voltage gain," *IEEE Trans. Ind. Electron.*, vol. 56, no. 8, 3144–3152, Aug. 2009.
32. N. Pogaku, M. Prodanovic, and T. C. Green, "Modeling, analysis and testing of autonomous operation of an inverter-based microgrid," *IEEE Trans. Power Electron.*, vol. 22, no. 2, pp. 613–625, Mar. 2007.

Published By:
Blue Eyes Intelligence Engineering and Sciences Publication (BEIESP)

Published By:
Blue Eyes Intelligence Engineering
and Sciences Publication (BEIESP)